Development of a double skin facade system applied in a virtual occupied chamber

inventions

MDPI

Article

Development of a Double Skin Facade System Applied in a Virtual Occupied Chamber

Eusébio Conceição [1,*], João Gomes [2], Maria Manuela Lúcio [1] and Hazim Awbi [3]

[1] Faculdade de Ciências e Tecnologia–Universidade do Algarve, Campus de Gambelas, 8005-139 Faro, Portugal; maria.manuela.lucio@gmail.com
[2] CINTAL, Campus de Gambelas, 8005-139 Faro, Portugal; jgomes@ualg.pt
[3] School of Construction Management & Engineering, University of Reading, Reading RG6 6AW, UK; h.b.awbi@reading.ac.uk
* Correspondence: econcei@ualg.pt; Tel.: +351-289-800-900

Abstract: In this study a system constituted by seven double skin facades (DSF), three equipped with venetian blinds and four not equipped with venetian blinds, applied in a virtual chamber, is developed. The project will be carried out in winter conditions, using a numerical model, in transient conditions, and based on energy and mass balance linear integral equations. The energy balance linear integral equations are used to calculate the air temperature inside the DSF and the virtual chamber, the temperature on the venetian blind, the temperature on the inner and outer glass, and the temperature distribution in the surrounding structure of the DSF and virtual chamber. These equations consider the convection, conduction, and radiation phenomena. The heat transfer by convection is calculated by natural, forced, and mixed convection, with dimensionless coefficients. In the radiative exchanges, the incident solar radiation, the absorbed solar radiation, and the transmitted solar radiation are considered. The mass balance linear integral equations are used to calculate the water mass concentration and the contaminants mass concentration. These equations consider the convection and the diffusion phenomena. In this numerical work seven cases studies and three occupation levels are simulated. In each case the influence of the ventilation airflow and the occupation level is analyzed. The total number of thermal and indoor air quality uncomfortable hours are used to evaluate the DSF performance. In accordance with the obtained results, in general, the indoor air quality is acceptable; however, when the number of occupants in the virtual chamber increases, the Predicted Mean Vote index value increases. When the airflow rate increases the total of Uncomfortable Hours decreases and, after a certain value of the airflow rate, it increases. The airflow rate associated with the minimum value of total Uncomfortable Hours increases when the number of occupants increases. The energy production decreases when the airflow increases and the production of energy is higher in DSF with venetian blinds system than in DSF without venetian blinds system.

Keywords: double skin facade; virtual chamber; numerical simulation; thermal comfort; indoor air quality

Citation: Conceição, E.; Gomes, J.; Lúcio, M.M.; Awbi, H. Development of a Double Skin Facade System Applied in a Virtual Occupied Chamber. *Inventions* **2021**, *6*, 17. https://doi.org/10.3390/inventions6010017

Academic Editor: Ping-Hei Chen

Received: 21 December 2020
Accepted: 26 February 2021
Published: 4 March 2021

1. Introduction

A double skin facade (DSF) is usually made up of a transparent glass envelope that overlaps the building's common envelope, leaving an air cavity between these two facades ("skins"). In this air cavity, shading devices (usually of venetian-type blind) or systems that produce electrical energy such as photovoltaic cells can be installed. The air ventilation in the cavity can be controlled by natural processes or by mechanical or hybrid (using fans) processes [1]. The characteristics of the DSF depend on the facade typology, skin coverage, air ventilation strategies, shading devices integration, and use and location of the building, among others [2].

In recent years, much research has been conducted on DSF; namely, on its characteristics, use, performance, efficiency, and economic benefits. In the well-detailed work of

Ghaffarianhoseini et al. on the benefits and economic feasibility of the DSF use [1], the impact on thermal behavior, energy efficiency, and daylighting performance of the buildings of several DSF technical characteristics were analyzed. The authors concluded that, in general, DSFs are a technical option that create energy savings and improve the energy performance of buildings in a sustainable way, as well as contributing to the architecture of buildings being more pleasant [1]. Referring to other articles, Ghaffarianhoseini et al. [1] point out the environmental and economic benefits achieved with the use of DSF; namely, the energy consumption reduction, airflow and thermal comfort enhancement, daylighting and glare control, sound insulation, noise reduction and acoustic enhancement, visual and aesthetic quality enhancement, and reduced long term-cost. However, these benefits are not easily accounted for, depending essentially on having a very well designed and ventilated DSF, and largely depending on climatic conditions. The authors also note that there is still little knowledge about the overall performance of DSF, especially with regard to strategies for controlling their thermal behavior [1].

The efficacy of DSF depends on the detailed conditions of each specific situation in which it is applied, and its evaluation must be done for that specific case. In the design of the DSF it is impossible to define general rules for its optimization in relation to the entire building energy concept, which makes it important to numerically study the performance of DSF before their implementation in buildings. Thus, the performance of the DSF integrated in the performance of the building itself can be evaluated, in terms of energy efficiency, throughout the design project by the architects and engineers involved. The simulation of DSF performance can be done by using building energy simulation tools such as those presented in the review work of Lucchino et al. [3]. These building energy simulations are relatively flexible tools for the analysis of DSF systems, as different configurations can be modelled and simulated within the same environment. Regarding the DSF, the characteristics of these simulation tools were compared in their most relevant aspects (airflow, coefficients, and shading devices within, among others) in detail in the work of Lucchino et al. [3].

In naturally ventilated DSF it is very important to have an accurate assessment of the airflow for an adequate design and performance evaluation. For example, Xue and Li [4] developed a new fast and accurate computational fluid dynamics model which can be applied in optimal design of a DSF with natural air ventilation and in the analysis of its thermal performance. In order to have a better understanding of the thermal behavior of a DSF naturally ventilated with an incorporated venetian blind, a simple method based on tracer gas measurements and so-called determined "global discharge coefficients" was experimentally developed [5].

The use of shading devices within the air cavity of the DSF can provide protection against direct solar radiation and some isolation from the transmission of sound into the building [6,7]. The work of Hazem et al. [6] shows that, for a slat angle of the shading device of 0°, the direct solar radiation varies between 40 W/m^2 and 340 W/m^2 for an incidence angle of, respectively, 60° and 0°. For a slat angle of the shading device of 45°, the direct solar radiation varies between 20 W/m^2 and 140 W/m^2 for the same range of incidence angle. For a slat angle of the shading device of 85°, the direct solar radiation is around 20 W/m^2 for the same range of incidence angle. The work of Lee and Chang [7] shows that vertical shading devices with 30 mm thick and 75° worked as an efficient acoustic barrier at high frequencies with a transmission loss between 80 dB and 120 dB. The blinds' geometry influences the DSF cavity air temperature, air velocity, and airflow behavior, which in turn will affect the thermal and energy saving DSF performance [7,8]. Air cavity dimensions, orientation, and material properties (reflection, absorbance, and transmission) are aspects that determine the geometry of the blinds. The DSF thermal performance can be improved by using materials such as dielectric film coatings or pastel paints [9] and the insertion of Phase Change Materials (PCM) in the construction of the blinds [10]. These blinds with embodied phase change materials are thermally more efficient than aluminum blinds, with an outlet temperature difference of about 2.6 °C [10]. In the blinds can also be applied

photovoltaic cells. As an example, see the work of Luo et al. [11], which proved that it is possible to have significant heating energy gains in winter conditions with the use of a DSF system with photovoltaic cells blinds embedded. The heat gain of this system could be on average 73.74% higher than conventional DSF in winter. The article of Xu et al. [12] presents the advantages of combining DSF with photovoltaics cells and the impacts of ventilation strategies on DSF with photovoltaic performance. For example, in winter conditions, with no ventilation the average heat gain U is 3.4 W/m^2K and the electric efficiency is 5.3%, with natural ventilation U is 3.8 W/m^2K and the electric efficiency is 5.5%, and with mechanical ventilation U is 4.6 W/m^2K and the electric efficiency is 5.6%. The authors also pointed out that climate and regional adaptability of this kind of system should be taken into account [12].

The thermal and energy performance of DSF buildings are influenced by some parameters such as building orientation, glazing type, cavity width, and climatic conditions, as well as by the use of photovoltaic cells, phase change materials or venetian blinds, and by air ventilation mode option [13–18]. Proper DSF integration with PCM leads to up to 10.38% of building energy savings [13]. In the work of Fazelpour et al. [14], it was found that with the increase in cavity width from 0.4 to 1.2 m, the annual electricity consumption is reduced by 5.88, 5.19, and 7.49 MWh for Tehran, Tabriz, and Kish, respectively. When the slat angle is adjusted from 0° to 90° the temperature of the inner glazing reduces 1 °C at least [16]. For air layers intending to improve ventilation capacity, the channel width should not be higher than 0.6 m, while for those with the purpose of supplying warm air, the width should be lower than 0.2 m [17]. Increments between interior and surface temperatures of around 10 °C were observed for perforated layers [18]. Regarding the work of Kim et al. [19], it was shown that energy consumption and thermal loads in buildings can be reduced by around 52% and 27%, respectively, by applying adequate control strategies (as simple as blind raise/lower controls and daylight-based dimming) to DSF with external or internal incorporated blinds. Lee and Park [20] proposed to use the response factor in the numerical prediction calculation of cooling or heating load of a building with DSF with accurate results on the case of cooling load. The authors show that the DSF with the blind system can save about 70.9% of the cooling load compared with the single skin façade [20]. Kuznik et al. [21] presented a numerical modelling of a DSF used to study the influence of airflow rates and venetian-type blind blades angles on heat transfer in DSF. The idea was to optimize both parameters to obtain the lowest possible value of the interior glazing temperature.

The comfort indexes PMV (Predicted Mean Vote) and PPD (Predicted Percentage of Dissatisfied), developed by Fanger [22], can be used to define the thermal comfort requirements for occupied rooms equipped with heating, ventilation, and air conditioning systems. These indexes were adopted by the international standards ISO 7730 [23] and ASHRAE Standard 55 [24], where three thermal comfort categories are defined: category A ($-0.2 \leq \text{PMV} \leq +0.2$), category B ($-0.5 \leq \text{PMV} \leq +0.5$), and category C ($-0.7 \leq \text{PMV} \leq +0.7$). As an example, the PMV and PPD indexes were applied to the multi-nodal human thermal comfort numerical model developed by Conceição et al. [25].

Usually, the assessment of indoor air quality and ventilation system is done by measurements of indoor CO_2 concentrations [26,27]. The relationship between CO_2 concentration and the airflow rate, under steady-state conditions, is presented in ASHRAE Standard 62.1 [28]. This standard refers to a value of CO_2 concentration below 1800 mg/m^3 as an acceptable level of indoor air quality [28]. As an example, see the works of Conceição et al. [29,30].

Warm and Cold Uncomfortable Hours are concepts that were introduced by Olesen and Parsons [31] and Van der Linden et al. [32]. They are used to compare indoor spaces with different thermal discomfort levels over a long period of occupation time. The parameters used to evaluate the long-term thermal comfort conditions are presented in the ISO 7730 standard [23]. Air Quality Uncomfortable Hours and Total Uncomfortable Hours due to thermal and air quality conditions are concepts that were introduced by Conceição et al. [33]. This long-term integral model, which aggregates the Warm Un-

comfortable Hours, the Cold Uncomfortable Hours, and the Air Quality Uncomfortable Hours, is used to obtain the airflow rate that simultaneously provides the best indoor air quality and thermal comfort levels in an occupied space. It was applied in a numerical study done in a university library to obtain the optimal airflow rate in winter and summer conditions [33].

In order to guarantee improvements in thermal comfort and ventilation of interior spaces and gains in energy consumption from the use of DSF, the literature refers to the need to have well-designed and ventilated DSF and, therefore, its performance, integrated together with the thermal performance of the building, must be previously evaluated using whole building thermal behavior simulation tools [1,3]. In the revised literature, the researchers essentially evaluate the thermal behavior of the DSF itself, the effect of the type of ventilation used, or the energy consumption gains obtained by the building. There is a lack of investigation of an integrated assessment of these three aspects and its effect on the thermal comfort of the occupants. In this context, the authors propose, using a whole building thermal behavior simulation tool that has been developed by themselves over the past two decades, to numerically evaluate the thermal comfort of the occupants, the indoor air quality, and the energy gains obtained with the use of the designed DSF system.

The aim of this study is to develop a DSF system, based on seven DSF, three equipped with venetian blinds and four not equipped with venetian blinds, applied in an occupied virtual chamber. The energy produced and the airflow promoted in the DSF system is used to improve the thermal comfort and the air quality level in an adjacent and occupied chamber. The influence of the airflow rate in the DSF system, the influence of the occupation level in the virtual chamber, and the influence of the internal venetian blinds in the DSF on the internal air temperature, as well as energy production, occupants' thermal comfort, indoor air quality, and total Uncomfortable Hours levels are analyzed.

2. Models and Methods

The numerical methods applied in this work, previously developed by the authors, are based on a building thermal response methodology [34,35]. In the work of Conceição and Lúcio [34], the building thermal response numerical model was presented and applied, while in the work of Conceição et al. [35], the solar radiation numerical model, the glass radiative proprieties numerical model, and the convection heat transfer coefficients were presented. The building thermal response numerical model was validated in winter conditions [36] and in summer conditions [37]. In these validations test buildings with complex topology were used.

This numerical model considers energy and mass balance linear integral equations, used in the calculation, in transient conditions, of the temperature field (of opaque and transparent bodies of the DSF system and virtual chamber) and of the mass field (of the air inside the DSF system and virtual chamber) for the water and contaminants.

The linear equations system, of first order integral equations, is resolved using the Runge-Kutta-Felberg method with error control.

In Figure 1, a scheme of the conductive (yellow), convective (orange), and radiative phenomena (red) verified in the DSF and virtual chamber is presented. It also shows the airflow topology with blue color.

The energy balance linear integral equations consider the convection, conduction. and radiation phenomena:

- The heat transfer by convection is calculated by natural, forced, and mixed convection, through the use of dimensionless coefficients. These coefficients are used in the surfaces of the glasses and the opaque bodies;
- The heat transfer by conduction is considered inside the opaque bodies' layers. In the present work the conduction is verified in the opaque surfaces, between the different layers;
- In the radiative heat exchanges, the incident solar radiation, the absorbed solar radiation (by glasses and opaque bodies), and the transmitted solar radiation (through the

glass) are considered. In the radiation phenomena the shading devices are considered. More details can be seen in the works of Conceição and Lúcio [38,39]. In Conceição and Lúcio [38] a curtain of trees used to improve the comfort level was applied, while in Conceição and Lúcio [39], a building structure shading device was also used to promote the comfort level improvement.

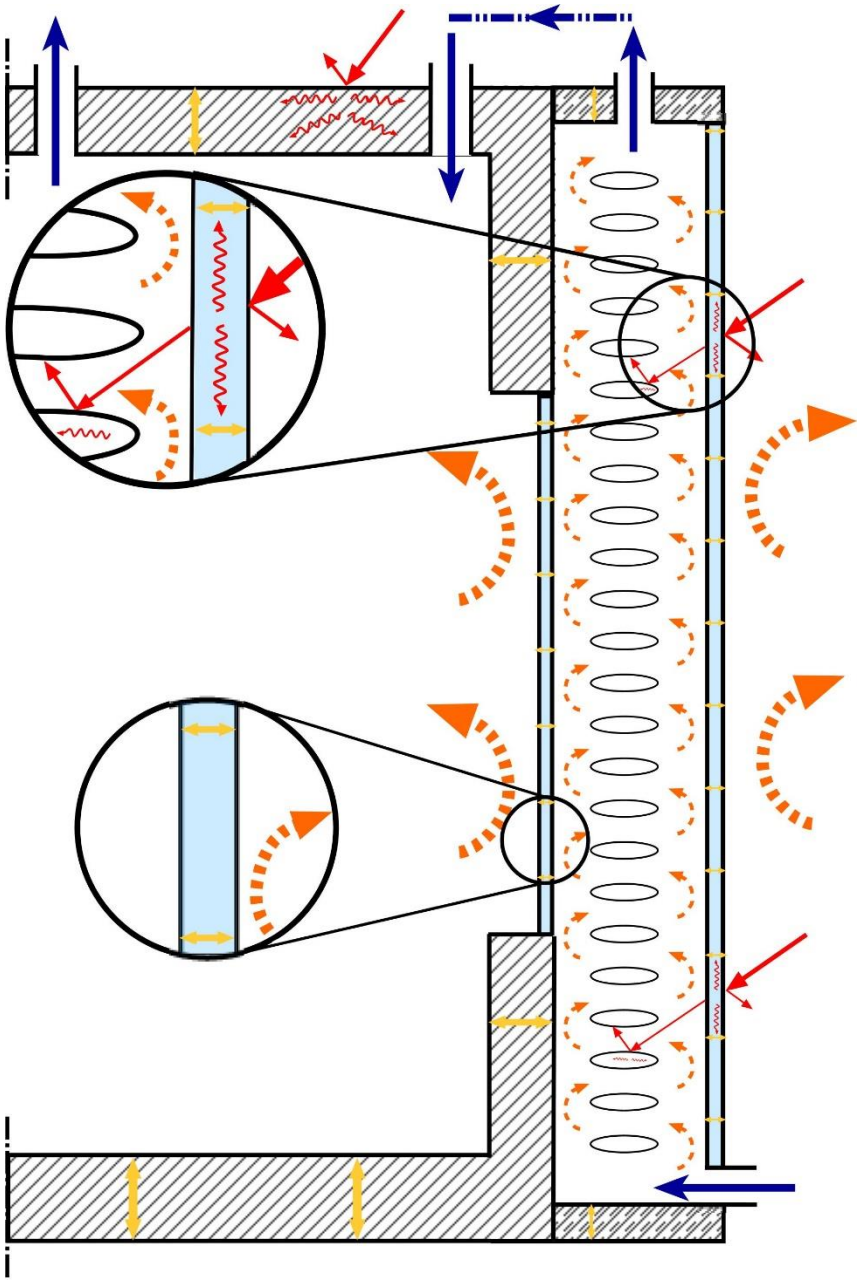

Figure 1. Scheme of the conductive (yellow), convective (orange) and radiative (red) phenomena and airflow (blue) topology verified in the double skin façades (DSF) and virtual chamber.

The energy balance linear integral equations are used to calculate the temperature of:

- The venetian blind, inner (window) and outer glass, surrounding structure of the DSF, and air inside the ventilated DSF;
- The opaque bodies (such as door, walls, floor, and ceiling), transparent bodies (such as glasses), indoor bodies (such as seat and desks), and internal air of the virtual chamber.

The mass balance linear integral equations are used to calculate the water mass concentration and the contaminants mass concentration. These equations consider the convection phenomenon.

The mass balance linear integral equations will be used in the calculation of the mass concentration of:

- Water vapor and contaminants concentration, such as the carbon dioxide concentration, inside the DSF;
- Water vapor and contaminants concentration, such as the carbon dioxide concentration, inside the virtual chamber.

In the inner glass, used as window, located between the virtual chamber and DSF spaces, the following energy phenomena are considered (see Figure 1):

- Convection between the glass surface and the air inside the DSF space and between the glass surface and the air inside the virtual chamber;
- Incident solar radiation, reflected solar radiation (to the DSF space), glass absorbed, and transmission solar radiation to the chamber space.

In the outer glass, located between the DSF space and outdoor environment, the following energy phenomena are considered (see Figure 1):

- Convection between the glass surface and the air inside the DSF space and between the glass surface and the outdoor environment;
- Incident solar radiation, reflected solar radiation (to the outdoor environment), glass absorbed and transmission solar radiation to the DSF space.

In the venetian blind, located inside the DSF space, the following energy phenomena are considered (see Figure 1):

- Convection between the venetian blind surfaces and the air inside the DSF space;
- Conduction between the upper and lower venetian blind, between adjacent layers in contact;
- Incident solar radiation, reflected solar radiation (to the DSF space), and absorption solar radiation.

In the opaque surface, as surrounding structure of the DSF and virtual chamber (door, walls, floor, and ceiling), the following energy phenomena are considered (see Figure 1):

- Convection between the inner and outer opaque surfaces and the surrounding air (chamber, DSF, or outdoor environment);
- Conduction in the opaque body between adjacent layers in contact;
- Incident solar radiation, reflected solar radiation (to the DSF space or outdoor environment), and absorption solar radiation.

In the air inside the DSF space, the following energy phenomena are considered (see Figure 1):

- Convection between DSF surrounding surfaces (DSF opaque structure, venetian blind, indoor window, and outdoor glass) system and the air inside the DSF space;
- Airflow forced convection from the outdoor environment to the DSF space;
- Airflow forced convection from the DSF space to the virtual chamber space.

In the air inside the virtual chamber spaces, the following energy phenomena are considered (see Figure 1):

- Convection between the surrounding surfaces (door, walls, floor, ceiling, and window) of the virtual chamber and the air inside the virtual chamber;
- Airflow forced convection from the DSF space to the virtual chamber space;
- Airflow forced convection from the virtual chamber space to the outdoor environment.

In the carbon dioxide concentration and the water vapor concentration inside the DSF space, the following mass phenomena are considered (see Figure 1):

- Airflow forced convection from the outdoor environment to the DSF space;
- Airflow forced convection from the DSF space to the virtual chamber space;

In the carbon dioxide concentration and the water vapor concentration inside the chamber spaces the following mass phenomena are considered (see Figure 1):

- Airflow forced convection from the DSF space to the virtual chamber space;
- Airflow forced convection from the chamber space to the outdoor environment space.

This numerical model also allows the calculation, among other variables, of the DSF and virtual chamber bodies, the DSF and virtual chamber internal air temperatures, the PMV and PPD indexes, and the carbon dioxide concentration inside the DSF and virtual chamber. The PMV and the PPD indexes evaluation, used in this software, are applied in more detail in Conceição et al. [40].

The projected virtual chamber (see Figure 2) has the dimensions presented in Table 1. It is made of wood and insulated with extruded polystyrene material with a thickness of 40 mm. The virtual chamber, similar to the existing experimental chamber, is built with square-section bars that support square modules. It consists of 108 square modules of 60×60 cm^2 distributed as follows: 28 modules in each side wall and ceiling; 16 modules in the rear wall; and 8 modules in the front wall. The virtual chamber is equipped with two doors, each one with 0.6 m by 2.5 m dimensions, and three windows installed inside the DSF system, each one with 0.6 m by 1.2 m dimensions.

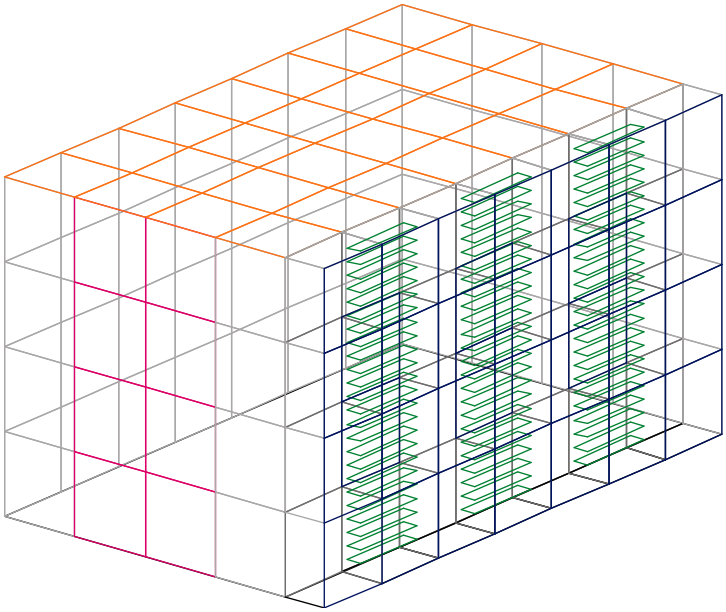

Figure 2. Virtual chamber equipped with seven DSF installed in the south-facing envelope. In blue are represented the transparent glasses, in green are represented the venetian blinds, in grey are represented the opaque walls, in red is presented the door, in orange is presented the ceiling, and in black is presented the floor.

Table 1. Dimensions of the main elements.

Element	Length (m)	Width (m)	Height (m)	Thickness (mm)
Virtual Chamber	4.50	2.55	2.5	-
DSF	0.60	0.2	2.5	-
Lamella	0.60	0.12	-	10

The DSF system, built with seven DSF (see Figure 3), subjected to solar radiation, has the dimensions presented in Table 1. The DSF system is installed in the virtual chamber envelope facing south. Three DSF are equipped with a venetian-type blinds and four are not. The DSF consists of two transparent surfaces (glasses), each one with a thickness of

4 mm and a surrounding structure. It has an adjustable set of 24 aluminum lamellae located between the transparent surfaces. The dimensions of each lamella are presented in Table 1.

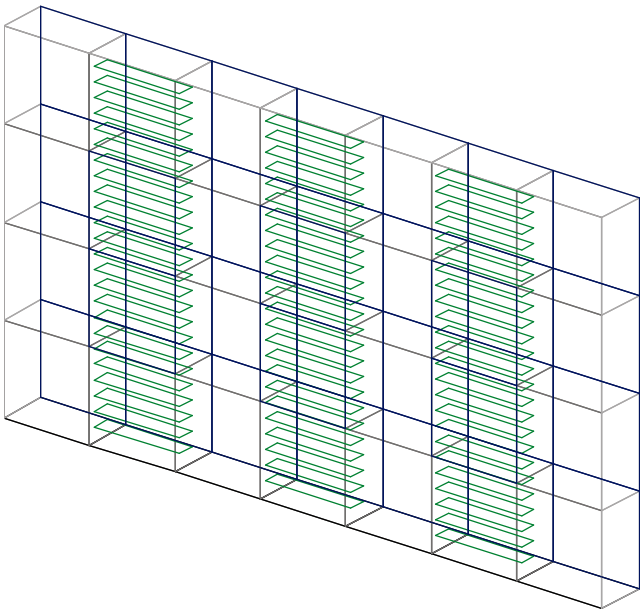

Figure 3. Seven DSF installed in the south-facing envelope. In blue are represented the transparent glasses, in green are represented the venetian blinds, in grey are represented the opaque walls, and in black is presented the floor.

In the numerical simulation an outdoor air temperature, air relative humidity, wind velocity, and wind direction were considered as input conditions. The numerical external conditions were measured on a typical winter day, in the south region of Portugal, obtained experimentally by a weather station located in the region. In these conditions, it was considered that the outdoor air temperature varied between 4.5 °C and 13.5 °C, the outdoor air relative humidity varied between 37.2% and 65%, and the wind speed varied between 0.01 m/s and 6.25 m/s.

The simulation was performed for 24 h considering clear sky. In terms of the solar radiation, a typical winter day, such as the 21st December, was used.

In this work seven cases were studied using three occupation levels (4, 8, and 12 persons) and considering seven airflows suggested by the standards for an occupation of 4, 8, 12, 16, 20, 24, and 28 persons (see Table 2).

Table 2. Cases studied: O refers to occupation and V to ventilation.

Case	Airflow Rate (m^3/s)	Number of Occupants		
		4	**8**	**12**
1	0.0389	O4V1	O8V1	O12V1
2	0.0778	O4V2	O8V2	O12V2
3	0.1167	O4V3	O8V3	O12V3
4	0.1556	O4V4	O8V4	O12V4
5	0.1944	O4V5	O8V5	O12V5
6	0.2333	O4V6	O8V6	O12V6
7	0.2722	O4V7	O8V7	O12V7

In Figure 2, the virtual chamber equipped with seven DSF installed in the south-facing envelope is presented, while in Figure 3 are presented the seven DSF installed in the south-facing envelope.

The virtual chamber has an occupation cycle between 8 (8 a.m.) and 12 h (12 p.m.) and between 14 (2 p.m.) and 18 h (6 p.m.) during the day. The metabolic rate of 1.2 met and the clothing insulation level of 1 clo were used in the determination of the PMV index [23].

In this simulation the perfect mixing system is considered. This type of system is associated with the outside air at the entrance mixing evenly with the air inside the compartment. Therefore, in the simulation, the exterior concentration of carbon dioxide at the entrance is uniformly mixed with the interior concentration of carbon dioxide and the concentration of carbon dioxide released by the occupants is also uniformly mixed with the concentration of carbon dioxide inside of the space. In this type of simulation, both the concentration of carbon dioxide and other variables, such as air temperature, air relative humidity, air velocity, and average radiant temperature, are uniform inside the compartment.

3. Results and Discussion

In this section the carbon dioxide concentration, the internal air temperature, the occupants Predicted Mean Vote, the Uncomfortable Hours, and the energy production are presented.

3.1. Indoor Air Quality

From Figures 4–6, the evolution of carbon dioxide concentration, for seven cases studied, is presented. The Figures 4–6 are associated with the virtual chamber occupied, respectively, by 4, 8 and 12 occupants.

In all figures, and in the next figures, the occupation time is represented, namely in the morning, between 8 a.m. and 12 p.m. and in the afternoon between 2 p.m. and 6 p.m.

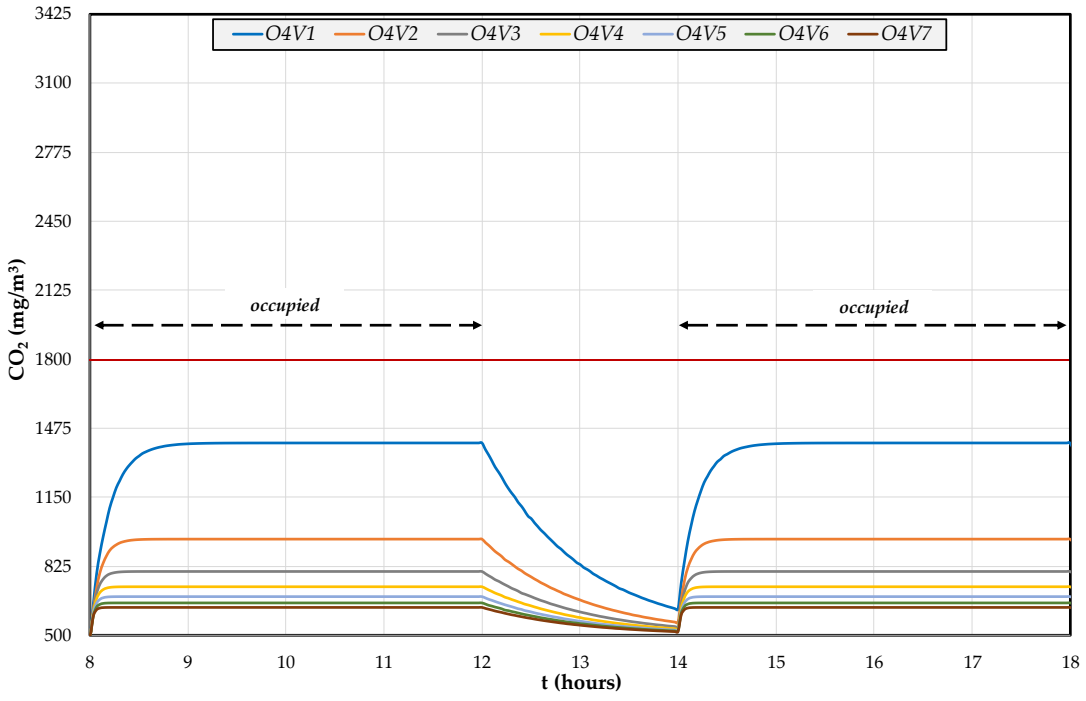

Figure 4. Evolution of carbon dioxide concentration (CO_2), for the seven cases studied, when the virtual chamber is occupied by four occupants. The red line represents the limit of acceptable indoor air quality [28].

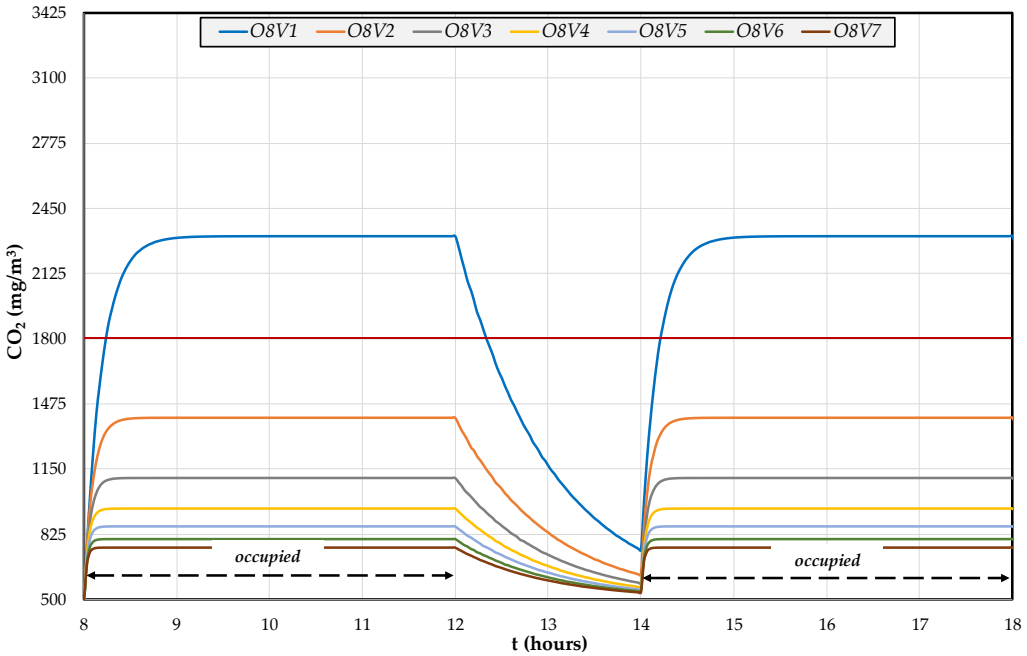

Figure 5. Evolution of carbon dioxide concentration (CO_2), for the seven cases studied, when the virtual chamber is occupied by eight occupants. The red line represents the limit of acceptable indoor air quality [28].

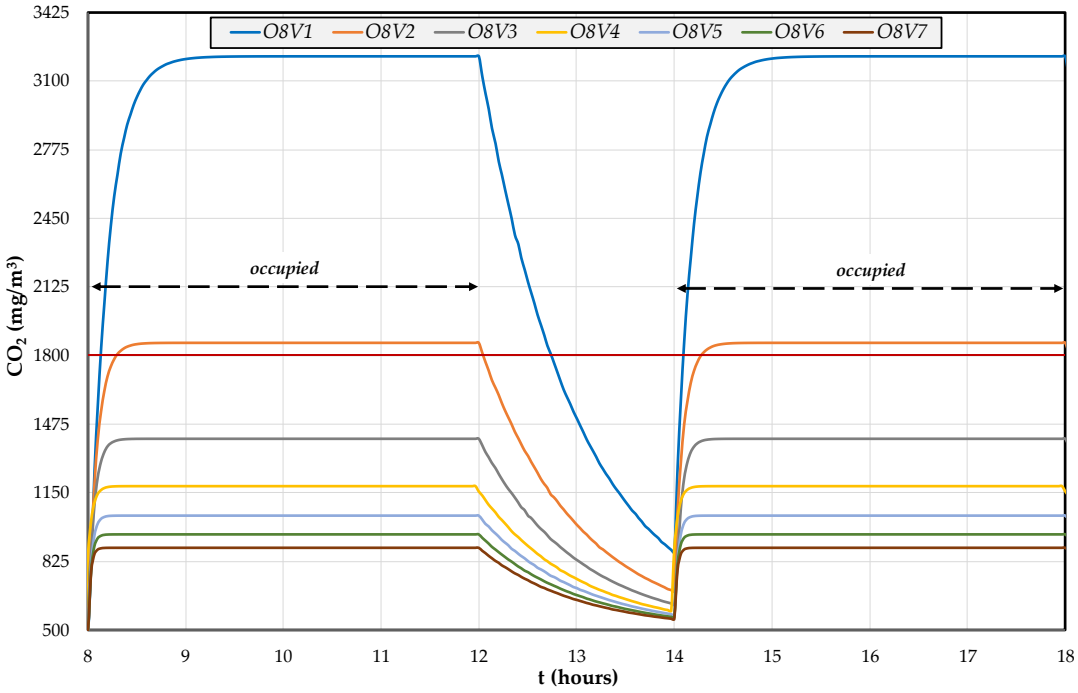

Figure 6. Evolution of carbon dioxide concentration (CO_2) for the seven cases studied, when the virtual chamber is occupied by 12 occupants. The red line represents the limit of acceptable indoor air quality [28].

The carbon dioxide concentration increases when the virtual chamber is occupied and decreases when the virtual chamber is not occupied. The carbon dioxide concentration increases when the occupation level increases and decreases when the airflow increases. When the virtual chamber is occupied by four occupants the carbon dioxide concentration is acceptable for all cases, when the virtual chamber is occupied by eight occupants the carbon dioxide concentration is not acceptable only for one case, while when the virtual chamber is occupied by 12 occupants the carbon dioxide concentration is not acceptable

for two cases. All not acceptable cases are verified when the airflow rate is lower than the airflow rate suggested by the standards.

3.2. Indoor Air Temperature

From Figures 7–9, the evolution of virtual chamber internal air temperature, for the seven cases studied, is presented. Figures 7–9 are associated with the virtual chamber occupied, respectively, by 4, 8 and 12 occupants.

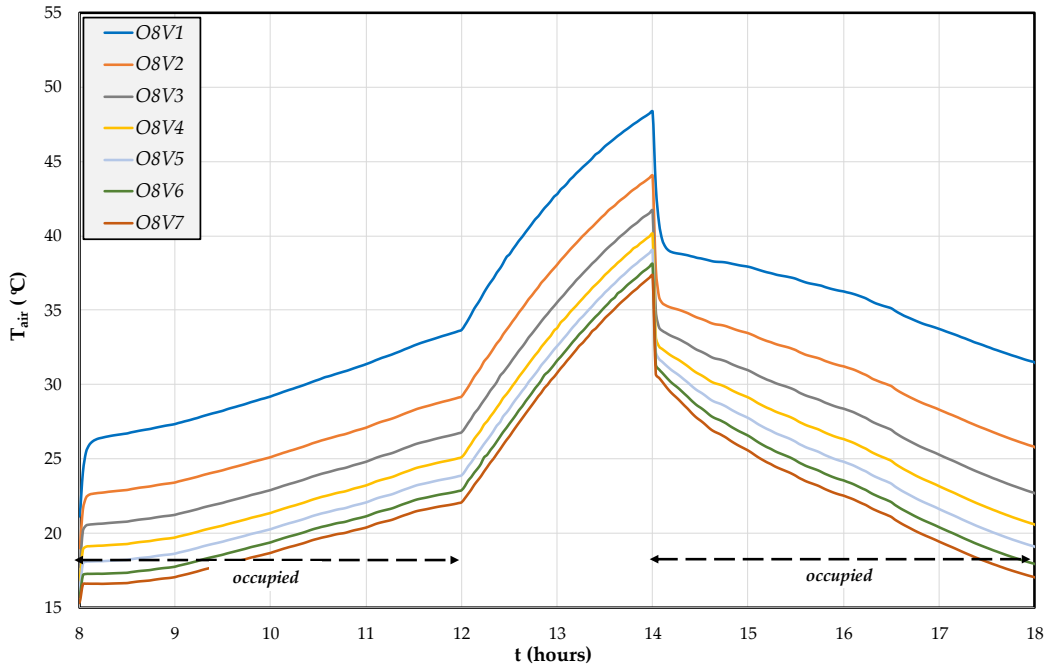

Figure 7. Evolution of virtual chamber internal air temperature, for the seven cases studied, when the virtual chamber is occupied by four occupants.

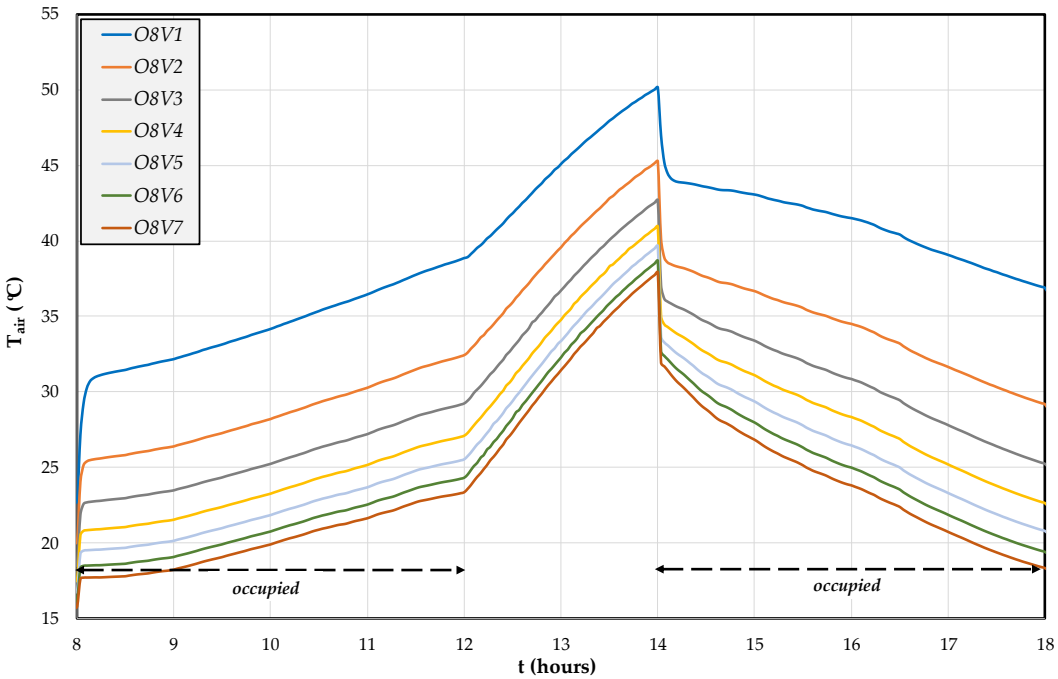

Figure 8. Evolution of virtual chamber internal air temperature, for the seven cases studied, when the virtual chamber is occupied by eight occupants.

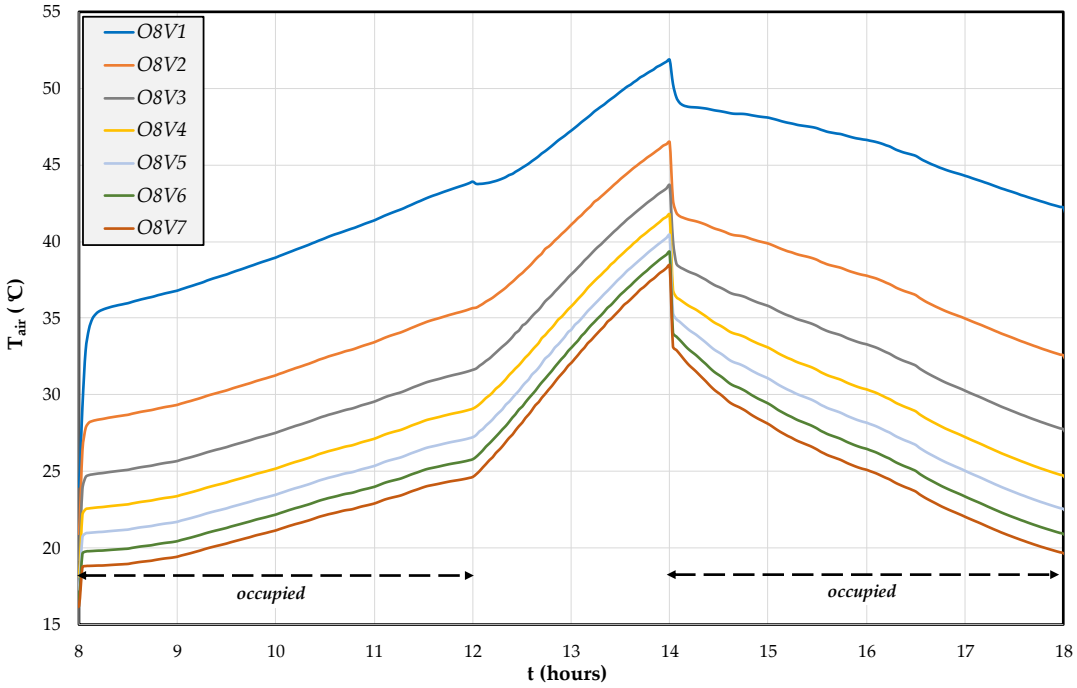

Figure 9. Evolution of virtual chamber internal air temperature, for the seven cases studied, when the virtual chamber is occupied by 12 occupants.

The virtual chamber internal air temperature increases in the morning and at lunch and decreases in the afternoon. The virtual chamber internal air temperature increase is associated with the increase of the solar radiation level and the decrease is associated with the decrease of the solar radiation level.

When the airflow rate increases the virtual chamber internal air temperature level also increases. When the occupants of the virtual chamber increase the virtual chamber internal air temperature level also increases.

3.3. Predicted Mean Vote Index

From Figures 10–12, the evolution of Predicted Mean Vote index, for the seven cases studied, is presented. The Figures 10–12 are associated with the virtual chamber occupied, respectively, by 4, 8, and 12 occupants. In the interrupted bold line is presented, from Figures 10–12, the limits of acceptable thermal comfort (Category C of the ISO 7730 [23]), namely the −0.7 (minimum acceptable thermal comfort level) and the +0.7 (maximum acceptable thermal comfort level).

The Predicted Mean Vote index, in general, increases in the morning and during lunch time and decreases during the afternoon. The increase is associated with the increase of virtual chamber internal air temperature and the decrease is associated with the decrease of virtual chamber internal air temperature.

The lowest airflow rate is associated with uncomfortable thermal comfort levels, by positive Predicted Mean Vote index; however, the highest airflow rate is associated with uncomfortable thermal comfort levels, by negative Predicted Mean Vote index, in the morning and is associated with comfortable thermal comfort levels, in general, in the afternoon. Middle airflow rates are associated, in general, with comfortable thermal comfort levels.

When the number of occupants in the virtual chamber increases the Predicted Mean Vote index value increases.

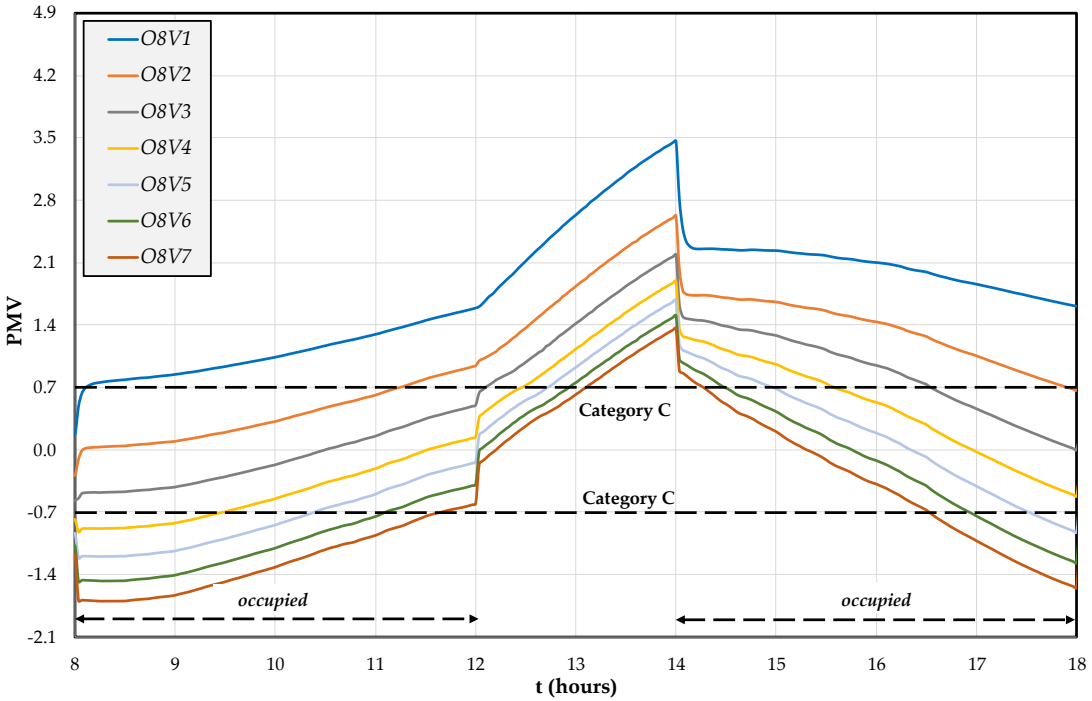

Figure 10. Evolution of Predicted Mean Vote (PMV) index, for the seven cases studied, when the virtual chamber is occupied by four occupants. The dashed lines represent the limits of Category C of ISO 7730 [23].

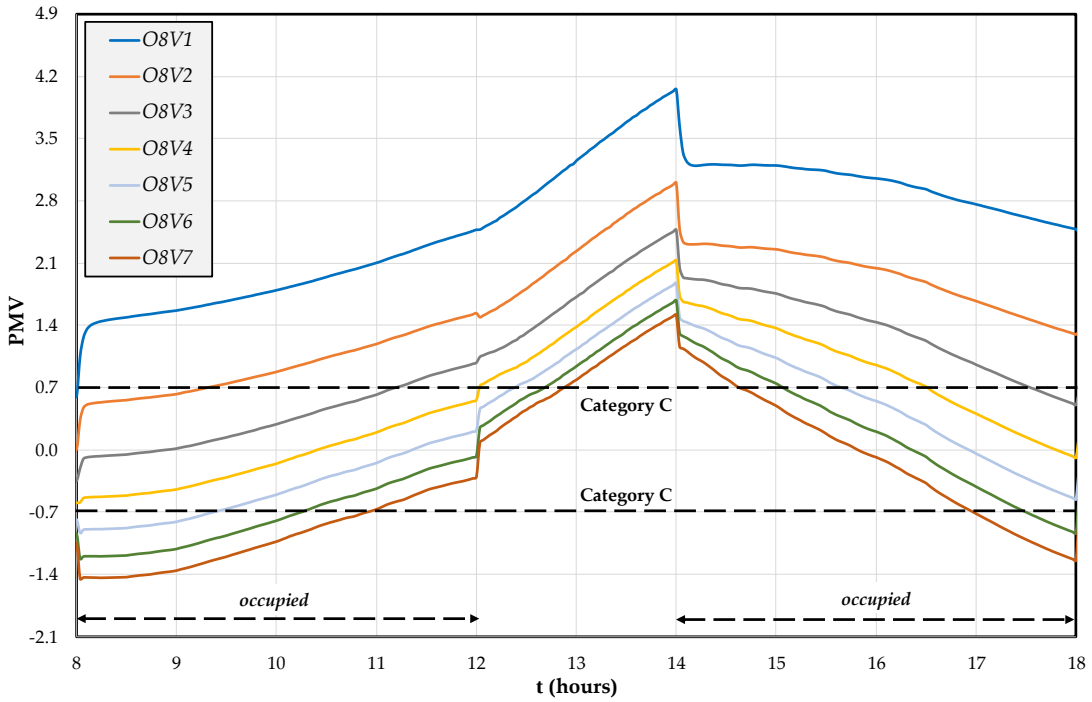

Figure 11. Evolution of Predicted Mean Vote (PMV) index, for the seven cases studied, when the virtual chamber is occupied by eight occupants. The dashed lines represent the limits of Category C of ISO 7730 [23].

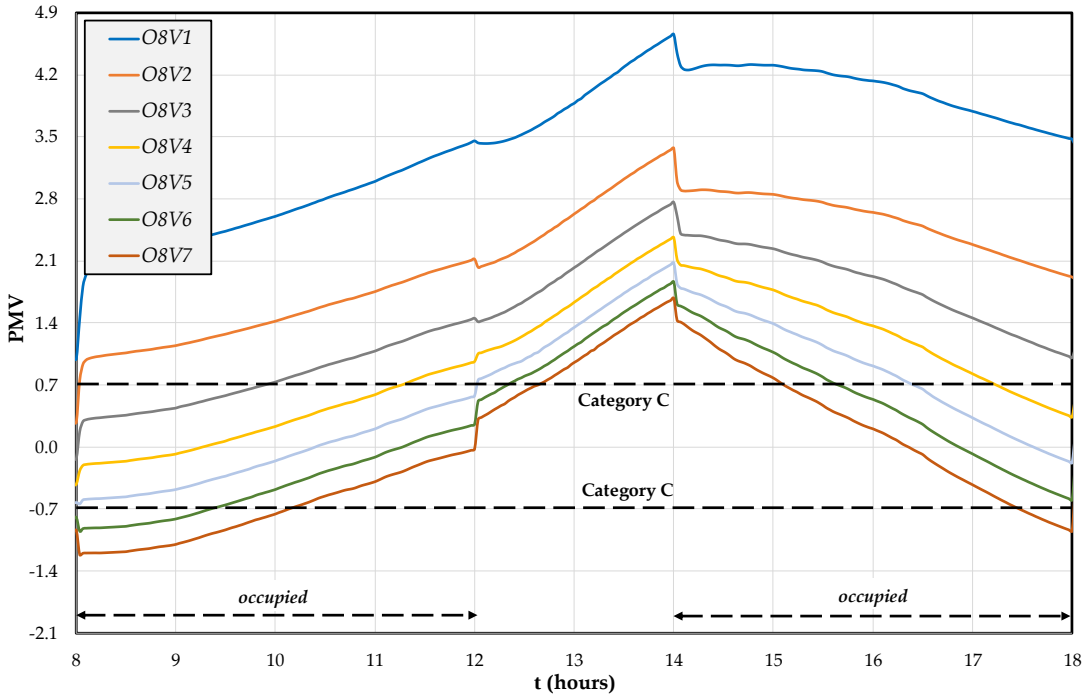

Figure 12. Evolution of Predicted Mean Vote (PMV) index, for the seven cases studied, when the virtual chamber is occupied by 12 occupants. The dashed lines represent the limits of Category C of ISO 7730 [23].

3.4. Uncomfortable Hours

From Tables 3–5 are presented the values of Cold Uncomfortable Hours (CUH), Warm Uncomfortable Hours (WUH), Air Quality Uncomfortable Hours (AQUH), and Uncomfortable Hours (UH) for each case studied. Table 3 is associated with an occupation of 4 persons, Table 4 is associated with an occupation of 8 persons, and Table 5 is associated with an occupation of 12 persons.

When the virtual chamber is occupied by four occupants and when the airflow rate increases the Cold Uncomfortable Hours increase and the Warm Uncomfortable Hours decrease. As the Air Quality Uncomfortable Hours is null, when the airflow increases, the Uncomfortable Hours decrease and after increase. Thus, a minimum of Uncomfortable Hours is verified for an airflow rate of 0.1556 m^3/s.

As was verified in the previous occupation level, when the virtual chamber is occupied by eight occupants, when the airflow rate increases the Cold Uncomfortable Hours decrease and the Warm Uncomfortable Hours increase. In the Air Quality Uncomfortable Hours only the first case is not null. Thus, the minimum of Uncomfortable Hours is verified for an airflow rate of 0.1944 m^3/s.

When the virtual chamber is occupied by 12 occupants, the same results of the previous two tests are verified. However, in this case, the Air Quality Uncomfortable Hours for the two first cases are not null and the minimum of the Uncomfortable Hours is verified for an airflow rate of 0.2333 m^3/s.

When the occupation in the virtual chamber increases, the Cold Uncomfortable Hours decrease, however the Warm Uncomfortable Hours and consequently the total Uncomfortable Hours increase. The airflow rate associated with the minimum value of total Uncomfortable Hours increases when the occupants number increases.

The Predicted Mean Vote index associated with low Uncomfortable Hours (see Tables 2–4 and Figures 10–12) presents an evaluation in general inside the acceptable thermal comfort area: in Figure 10 the Case 4, in Figure 11 the Case 5, and in Figure 12 the Case 6.

Table 3. Values of Cold Uncomfortable Hours (CUH), Warm Uncomfortable Hours (WUH), Air Quality Uncomfortable Hours (AQUH), and Uncomfortable Hours (UH) for each case, when the virtual chamber is occupied by four occupants.

Case	CUH	WUH	AQUH	UH
O4V1	0.00	28.74	0.00	28.74
O4V2	0.00	12.66	0.00	12.66
O4V3	0.00	5.95	0.00	5.95
O4V4	1.96	3.00	0.00	4.96
O4V5	5.08	1.56	0.00	6.65
O4V6	9.25	0.76	0.00	10.01
O4V7	13.64	0.41	0.00	14.05

Table 4. Values of Cold Uncomfortable Hours (CUH), Warm Uncomfortable Hours (WUH), Air Quality Uncomfortable Hours (AQUH), and Uncomfortable Hours (UH) for each case, when the virtual chamber is occupied by eight occupants.

Case	CUH	WUH	AQUH	UH
O4V1	0.00	44.23	8.77	53.00
O4V2	0.00	25.01	0.00	25.01
O4V3	0.00	12.70	0.00	12.70
O4V4	1.96	6.48	0.00	6.48
O4V5	3.55	1.85	0.00	5.40
O4V6	4.78	2.00	0.00	6.78
O4V7	8.52	1.08	0.00	9.60

Table 5. Values of Cold Uncomfortable Hours (CUH), Warm Uncomfortable Hours (WUH), Air Quality Uncomfortable Hours (AQUH), and Uncomfortable Hours (UH) for each case, when the virtual chamber is occupied by 12 occupants.

Case	CUH	WUH	AQUH	UH
O4V1	0.00	51.26	11.02	62.28
O4V2	0.00	37.75	7.56	45.31
O4V3	0.00	22.18	0.00	22.18
O4V4	0.00	11.97	0.00	11.97
O4V5	0.00	6.59	0.00	6.59
O4V6	1.85	3.83	0.00	5.68
O4V7	4.54	2.27	0.00	6.81

3.5. Energy Production

From Tables 6–8, the distribution daily thermal energy production, for the seven cases studied, is presented. The Tables 6–8 are associated with the virtual chamber occupied, respectively, by 4, 8 and 12 occupants.

The calculation of the energy production is associated with the airflow rate in the DSF system, the air specific heat, and the difference of temperature between the outdoor environment and the DSF indoor air. During the day, for each case studied the airflow rate was constant, however the air specific heat, the outdoor environment temperature, and the DSF indoor air temperature change during the day.

Table 6. Values of daily thermal energy production, for the seven cases studied, when the virtual chamber is occupied by four occupants.

Airflow Rate (m^3/s)	Thermal Energy Production by DSF with Blinds (kWh)	Thermal Energy Production by DSF without Blinds (kWh)	Thermal Energy Total Production (kWh)
0.0389	3.441	2.984	22.259
0.0778	2.476	2.166	16.094
0.1167	2.032	1.793	13.268
0.1556	1.770	1.573	11.599
0.1944	1.595	1.427	10.492
0.2333	1.468	1.321	9.685
0.2722	1.370	1.239	9.065

Table 7. Values of daily thermal energy production, for the seven cases studied, when the virtual chamber is occupied by eight occupants.

Airflow Rate (m^3/s)	Thermal Energy Production by DSF with Blinds (kWh)	Thermal Energy Production by DSF without Blinds (kWh)	Thermal Energy Total Production (kWh)
0.0389	3.504	3.017	22.578
0.0778	2.508	2.178	16.235
0.1167	2.056	1.799	13.365
0.1556	1.790	1.579	11.684
0.1944	1.611	1.431	10.558
0.2333	1.482	1.324	9.743
0.2722	1.383	1.242	9.118

Table 8. Values of daily thermal energy production, for the seven cases studied, when the virtual chamber is occupied by 12 occupants.

Airflow Rate (m^3/s)	Thermal Energy Production by DSF with Blinds (kWh)	Thermal Energy Production by DSF without Blinds (kWh)	Thermal Energy Total Production (kWh)
0.0389	3.548	3.035	22.783
0.0778	2.538	2.187	16.361
0.1167	2.084	1.810	13.491
0.1556	1.810	1.585	11.768
0.1944	1.629	1.436	10.634
0.2333	1.498	1.328	9.806
0.2722	1.397	1.246	9.173

The energy production increases during the morning and during lunch and decreases during the afternoon. This energy production is associated with the solar energy level. The energy production decreases when the airflow increases. The production of energy is higher in DSF equipped with a venetian blinds system than in DSF not equipped with a venetian blinds system.

The energy production increases slightly when the occupation increases. This fact is associated with the heat transmitted by conduction, through the wall, and between the DSF indoor air and the virtual chamber indoor environment. When the occupation level increases, the internal DSF indoor air temperature slightly increases and the energy production also slightly increases.

4. Conclusions

In this study the development of a DSF system applied in a virtual chamber is made. The DSF system is used in energy production, using the solar radiation, to improve the comfort level, namely the thermal comfort level, using the PMV index and the indoor air quality level, using the carbon dioxide concentration. This integral work considers seven airflow rates and three occupation levels.

When the number of occupants increases, the level of indoor air quality decreases. All unacceptable indoor air quality levels are verified when the airflow rate is lower than the airflow rate suggested by the standards.

When the number of occupants increases in the virtual chamber, the chamber internal air temperature level and the Predicted Mean Vote index value increases.

When the airflow rate increases the Cold Uncomfortable Hours decrease, the Warm Uncomfortable Hours increase, and the total Uncomfortable Hours decrease and then increase. The airflow rate associated with the minimum value of total Uncomfortable Hours increases when the occupants number increases.

The energy production decreases when the airflow increases. The production of energy is higher in DSF equipped with a venetian blinds system than in DSF not equipped with a venetian blinds system.

In accordance with the obtained results, the application of the DSF in the production of energy can be used to improve the indoor air quality and the thermal comfort levels to which the occupants are subjected. The indoor air quality is easier to guarantee, because it is only related to the airflow rate and the occupation level, rather than the thermal comfort level.

Thus, in order to guarantee an acceptable thermal comfort level in winter conditions during the entire day, it is necessary to apply control systems to the airflow rate or other variables. This is a new topic for future works. The application of the DSF system in summer conditions is also a new topic for future works.

Author Contributions: E.C., J.G., M.M.L. and H.A. contributed equally in the preparation of this manuscript. All authors have read and agreed to the published version of the manuscript.

Funding: The authors would like to acknowledge the project (SAICT-ALG/39586/2018) from Algarve Regional Operational Program (CRESC Algarve 2020), under the PORTUGAL 2020 Partnership Agreement, through the European Regional Development Fund (ERDF) and the National Science and Technology Foundation (FCT).

Institutional Review Board Statement: Not applicable.

Informed Consent Statement: Not applicable.

Data Availability Statement: Data sharing not applicable.

Conflicts of Interest: The authors declare no conflict of interest.

References

1. Ghaffarianhoseini, A.; Ghaffarianhoseini, A.; Berardi, U.; Tookey, J.; Li, D.; Kariminia, S. Exploring the advantages and challenges of double-skin façades (DSFs). *Renew. Sustain. Energy Rev.* **2016**, *60*, 1052–1065. [CrossRef]
2. Poirazis, H. *Double Skin Façades for Office Buildings—Literature Review*; Report EBD-R–04/3; Department of Construction and Architecture, Lund University: Lund, Sweden, 2004.
3. Lucchino, E.; Goia, F.; Lobaccaro, G.; Chaudhary, G. Modelling of double skin facades in whole-building energy simulation tools: A review of current practices and possibilities for future developments. *Build. Simul.* **2019**, *12*, 3–27. [CrossRef]
4. Xue, F.; Li, X. A fast assessment method for thermal performance of naturally ventilated double-skin façades during cooling season. *Sol. Energy* **2015**, *114*, 303–313. [CrossRef]
5. Silva, F.; Gomes, M.; Rodrigues, A. Measuring and estimating airflow in naturally ventilated double skin facades. *Build. Environ.* **2015**, *87*, 29–301.
6. Hazem, A.; Ameghchouche, M.; Bougriou, C. A numerical analysis of the air ventilation management and assessment of the behavior of double skin facades. *Energy Build.* **2015**, *102*, 225–236. [CrossRef]
7. Lee, J.; Chang, D. Influence on vertical shading device orientation and thickness on the natural ventilation and acoustical performance of a double skin façade. *Procedia Eng.* **2015**, *118*, 304–309. [CrossRef]

8. Lee, J.; Alshayeb, M.; Chang, D. A study of shading device configuration on the natural ventilation efficiency and energy performance of a double skin façade. *Procedia Eng.* **2015**, *118*, 310–317. [CrossRef]
9. Parra, J.; Guardo, A.; Egusquiza, E.; Alavedra, P. Thermal performance of ventilated double skin façades with venetian blinds. *Energies* **2015**, *8*, 4882–4898. [CrossRef]
10. Li, Y.; Darkwa, J.; Su, W. Investigation on thermal performance of an integrated phase change material blind system for double skin façade buildings. *Energy Procedia* **2019**, *158*, 5116–5123. [CrossRef]
11. Luo, Y.; Zhang, L.; Liu, Z.; Xie, L.; Wang, X.; Wu, J. Experimental study and performance evaluation of a PV-blind embedded double skin façade in winter season. *Energy* **2018**, *165*, 326–342. [CrossRef]
12. Xu, C.; Ma, X.; Yu, C. Photovoltaic double-skin façade: A combination of active and passive utilizations of solar energy. *Indoor Built Environ.* **2019**, *28*, 1013–1107. [CrossRef]
13. Ziasistani, N.; Fazelpour, F. Comparative study of DSF, PV-DSF and PV-DSF/PCM building energy performance considering multiple parameters. *Sol. Energy* **2019**, *187*, 115–128. [CrossRef]
14. Fazelpour, F.; Soltani, N.; Markarian, E.; Khezerloo, H. Impact of multiple parameters on energy performance of PV-DSF buildings. *Proceedings* **2018**, *2*, 1487. [CrossRef]
15. Fatnassi, S.; Abidi-Saad, A.; Maad, R.; Polidori, G. Numerical study of spacing and alternation effects of parietal heat sources on natural convection flow in a DSF-channel: Application to BIPV. *Int. J. Heat Mass Transf.* **2018**, *54*, 3617–3629. [CrossRef]
16. Wang, Y.; Chen, Y.; Li, C. Airflow modeling based on zonal method for natural ventilated double skin façade with Venetian blinds. *Energy Build.* **2019**, *191*, 211–223. [CrossRef]
17. Zhang, T.; Yang, H. Flow and heat transfer characteristics of natural convection in vertical air channels of double-skin solar façades. *Appl. Energy* **2019**, *242*, 107–120. [CrossRef]
18. Blanco, J.; Arriaga, P.; Rojí, E.; Cuadrado, J. Investigating the thermal behavior of double-skin perforated sheet façades: Part A: Model characterization and validation procedure. *Build. Environ.* **2014**, *82*, 50–62. [CrossRef]
19. Kim, D.; Cox, S.; Cho, H.; Yoon, J. Comparative investigation on building energy performance of double skin façade (DSF) with interior or exterior slab blinds. *J. Build. Eng.* **2018**, *20*, 411–423. [CrossRef]
20. Lee, S.; Park, J. Evaluating thermal performance of double-skin façade using response factor. *Energy Build.* **2020**, *209*, 109657. [CrossRef]
21. Kuznik, F.; Catalina, T.; Gauzere, L.; Woloszyn, M.; Roux, J.-J. Numerical modelling of combined heat transfers in a double skin façade—Full-scale laboratory experiment validation. *Appl. Therm. Eng.* **2011**, *31*, 3043–3054. [CrossRef]
22. Fanger, P. *Thermal Comfort: Analysis and Applications in Environmental Engineering*; Danish Technical Press: Copenhagen, Denmark, 1970.
23. ISO 7730. *Ergonomics of the Thermal Environments—Analytical Determination and Interpretation of Thermal Comfort Using Calculation of the PMV and PPD Indices and Local Thermal Comfort Criteria*; International Standard Organization: Geneva, Switzerland, 2005.
24. ANSI/ASHRAE Standard 55. *Thermal Environmental Conditions for Human Occupancy*; American Society of Heating, Refrigerating and Air-Conditioning Engineers: Atlanta, GA, USA, 2013.
25. Conceição, E.; Lúcio, M.; Awbi, H. Comfort and airflow evaluation in spaces equipped with mixing ventilation and cold radiant floor. *Build. Simul.* **2013**, *6*, 51–67. [CrossRef]
26. Asif, A.; Zeeshan, M.; Jahanzaib, M. Indoor temperature, relative humidity and CO_2 levels assessment in academic buildings with different heating, ventilation and air-conditioning systems. *Build. Environ.* **2018**, *133*, 83–90. [CrossRef]
27. Laverge, J.; Van Den Bossche, N.; Heijmans, N.; Janssens, A. Energy saving potential and repercussions on indoor air quality of demand controlled residential ventilation strategies. *Build. Environ.* **2011**, *46*, 1497–1503. [CrossRef]
28. ANSI/ASHRAE Standard 62-1. *Ventilation for Acceptable Indoor Air Quality*; American Society of Heating, Refrigerating and Air-Conditioning Engineers: Atlanta, GA, USA, 2016.
29. Conceição, E.; Farinho, J.; Lúcio, M. Evaluation of indoor air quality in classrooms equipped with cross-flow ventilation. *Int. J. Vent.* **2012**, *11*, 53–68. [CrossRef]
30. Conceição, E.; Lúcio, M.; Vicente, V.; Rosão, V. Evaluation of local thermal discomfort in a classroom equipped with cross flow ventilation. *Int. J. Vent.* **2008**, *7*, 267–277. [CrossRef]
31. Olesen, B.; Parsons, K. Introduction to thermal comfort standards and to the proposed new version of EN ISO 7730. *Energy Build.* **2002**, *34*, 537–548. [CrossRef]
32. Van der Linden, K.; Boerstra, A.; Raue, A.; Kurvers, S. Thermal indoor climate building performance characterized by human comfort response. *Energy Build.* **2002**, *34*, 737–744. [CrossRef]
33. Conceição, E.; Gomes, J.; Awbi, H. Influence of the airflow in a solar passive building on the indoor air quality and thermal comfort levels. *Atmosphere* **2019**, *10*, 766. [CrossRef]
34. Conceição, E.; Lúcio, M. Numerical simulation of passive and active solar strategies in building with complex topology. *Build. Simul.* **2010**, *3*, 245–261. [CrossRef]
35. Conceição, E.; Silva, M.; André, J.; Viegas, D. Thermal behaviour simulation of the passenger compartment of vehicles. *Int. J. Veh. Des.* **2000**, *24*, 372–387. [CrossRef]
36. Conceição, E.; Silva, A.; Lúcio, M. Numerical Study of Thermal Response of School Buildings in Winter Conditions. In Proceedings of the 9th Conference on Air Distribution in Rooms (Roomvent 2004), Coimbra, Portugal, 5–8 September 2004.
37. Conceição, E.; Lúcio, M. Numerical Study of Thermal Response of School Buildings in Summer Conditions. In Proceedings of the 8th International Conference and Exhibition on Healthy Buildings (HB 2006), Lisbon, Portugal, 4–8 June 2006.

38. Conceição, E.; Lúcio, M. Numerical study of the influence of opaque external trees with pyramidal shape in the thermal behaviour of a school building in summer conditions. *Indoor Built Environ.* **2010**, *19*, 657–667. [CrossRef]
39. Conceição, E.; Lúcio, M. Numerical study of the thermal efficiency of a school building with complex topology for different orientations. *Indoor Built Environ.* **2008**, *18*, 41–51. [CrossRef]
40. Conceição, E.; Gomes, J.; Ruano, A. Application of HVAC systems with control based on PMV index in university buildings with complex topology. *IFAC PapersOnLine* **2018**, *51*, 20–25. [CrossRef]